RSC Advances

PAPER

View Article Online
View Journal | View Issue

Cite this: *RSC Adv.*, 2025, **15**, 26000

Label-free biosensing of microRNA-423-5p in saliva sample of patients using KAUST catalysis center-1 modified dendritic AuNPs: a new platform towards early-stage diagnosis of oral cancer†

Hamed Bahari,[ab] Mohammad Hasanzadeh,*[b] Soodabeh Davaran,*[a] Farzin Ahmadpour[c] and Nasrin Shadjou[d]

Oral squamous cell carcinoma (OSCC) is the most prevalent form of oral cavity cancer and a leading cause of death globally with low survival rates. Early detection of OSCC is crucial for reducing morbidity and mortality. The microRNA-423-5p, a 23-nucleotide non-coding RNA, is a vital biomarker for accurate OC detection due to its high value in the Receiver Operating Characteristic (ROC) curve, ensuring selectivity for OC. A precise measurement of microRNA-423-5p in human biofluids facilitates accurate OC detection. This research introduces a novel electrochemical platform without the need for labeling, designed for the non-intrusive monitoring of microRNA-423-5p in human saliva samples using a DNA-based bioassay. In this approach, poly(β-cyclodextrin) was fabricated to serve as a biocompatible support on the glassy carbon electrode surface. Furthermore, KCC-1-nPr-NH-Arg, featuring a surface area of 104.9 $m^2\ g^{-1}$ and a pore volume of 0.83 $cm^3\ g^{-1}$, was utilized to enhance the substrate's surface area relative to volume and achieve high loading of probe DNA (pDNA). For the first time, dendritic AuNPs were used to immobilize thiolated DNA sequences (5′-SH-TGTCTCCCCGGTGTCTGGCTCGA-3′) on an electrode surface of electrode *via* Au–S interaction to detect microRNA-423-5p in human saliva in low limit of quantification of 1 pM. The biosensor successfully detected microRNA-423-5p, demonstrating its potential for OC screening. The genosensor development involved assessing crucial factors such as hybridization time and microRNA concentration. Analytical techniques including cyclic voltammetry, chronoamperometry, and differential pulse voltammetry were used for quantifying MicroRNA-423-5p in human biofluids. The biosensor's performance characteristics were evaluated for stability, repeatability, and suitability for plasma and saliva samples.

Received 25th May 2025
Accepted 15th July 2025

DOI: 10.1039/d5ra03672k

rsc.li/rsc-advances

1. Introduction

Oral cancer (OC) manifests as a diminutive, unknown, inexplicable lesion or ulceration in the oral cavity, including the cheeks, tongue, lips, hard and soft palate, and sinuses, as well as the base of the mouth extending to the oropharynx. OC is positioned as the sixth most prevalent form of cancer worldwide.[1] OC is generally regarded as the fourth most prevalent cancer in men and the eighth most common cancer in women.[2] It causes 3.8% of all cancer cases overall and 3.6% of cancer mortalities.[3] Oral squamous cell carcinoma (OSCC) is responsible for 95% of oral cancer cases, resulting in around 145 000 deaths worldwide each year. This high incidence of OSCC contributes to significant mortality and morbidity rates. The first stages of OSCC have an encouraging outlook, with a cure rate of 80% in the initial stage and 65% in the second stage. Despite significant advancements in treatment, the 5 years survival rate for most malignancies is still around 50% since they are typically discovered at late stages III or IV. Therefore, early detection of OSCC is crucial to lowering its morbidity and mortality.[2]

Visual inspection and various biopsy[4–7] are the mainstays of traditional approaches for the detection of OC and premalignant lesions (such as erythroplakia and leukoplakia). Currently, a tissue biopsy of the affected area is used to make the early analysis of OC. This is followed by additional evaluation using medical imaging techniques, such as expensive and difficult

[a]*Department of Medical Nanotechnology, Faculty of Advanced Medical Sciences, Tabriz University of Medical Sciences, Tabriz, 516661-4733, Iran. E-mail: davaran@tbzmed.ac.ir*

[b]*Pharmaceutical Analysis Research Center, Tabriz University of Medical Science, Tabriz, Iran. E-mail: hasanzadehm@tbzmed.ac.ir*

[c]*Department of Oral and Maxillofacial Surgery, Dentistry Faculty, Tabriz University of Medical Sciences, Tabriz, Iran*

[d]*Department of Nanotechnology, Faculty of Chemistry, Urmia University, Urmia, Iran*

† Electronic supplementary information (ESI) available. See DOI: https://doi.org/10.1039/d5ra03672k

positron emission tomography (PET) scans, magnetic resonance imaging (MRI),[8–10] or computed tomography (CT).[11–14]

Non-coding RNAs (ncRNAs)[15] are transcripts that are not involved in the coding of proteins. They are classified into two categories: short non-coding RNAs, which are less than 200 nt, and long non-coding RNAs, which are more than 200 nt.[16,17] NcRNAs make up the majority of the transcriptome, and intriguingly, their abundance is inversely correlated with organismal complexity.[18]

The shorter primordial miRNA (pri-miRNA) transcripts, which have one or more hairpins, give rise to miRNAs, which are RNAs with a length of 22 nucleotides or less. Few miRNA hairpins overlap protein-coding gene exons; the majority come from non-coding introns or transcripts.[19]

There is a chance that possible disease indicators may enter this fluid given that oral malignancies develop in the oral cavity. In order to do this, new research have proposed using salivary miRNAs as biomarkers for cancer diagnosis. Saliva collection is simple,[20] noninvasive, and does not require expensive trained employees or involved processes, which is a benefit.[3]

MicroRNA-423-5p was chosen as a diagnostic biomarker of oral cancer due to the high level under the chart in the Receiver Operating Characteristic (ROC) curve based on the ref. 21. ROC curve is used to evaluate the comprehensive diagnostic efficacy of a test and to evaluate the efficacy of two or more diagnostic tests. Additionally, it is employed to choose an ideal threshold for identifying the existence or non-existence of a disease.[22] Patients with recently discovered untreated main healthy controls and OSCC had their saliva collected. A microarray method was used to profile salivary miRNAs globally, and quantitative real-time PCR (RT-qPCR) was used to validate the signatures. For the standardization of RT-qPCR data and microarray, a rigorous statistical methodology was used. An extensive analysis was conducted to evaluate the diagnostic efficacy of miRNAs and their association with the prediction of OSCC. Among healthy controls and OSCC patients, 25 miRNAs indicated differential expression, and seven of these were found to be substantially linked with disease-free survival (DFS). Saliva from OSCC patients had significant levels of miR-423-5p, miR-193b-3p and miR-106b-5p expression, and their mixture exhibits the greatest diagnostic efficacy (ROC − AUC = 0.98). Additionally, strong expression of microR-423-5p was an independent predictor of poor DFS when included in multivariate survival analysis with the number of positive lymph nodes, the only significant clinical prognosticator. Finally, they founded that the expression of microR-423-5p was much lower in matching post-operative saliva samples, indicating that it may have originated specifically in malignancy.[21] So, microR-423-5p is suitable biomarker for the efficient recognition of OC by analysis of saliva samples of patient.

Recently, biosensor technology was widely used for the bioanalysis of cancer biomarker. Electrochemical biosensors have emerged as very effective and advanced devices in the field of biomedical diagnostics.[23] The key components integral to these biosensors are the signal transducer and the biorecognition element.[23] When compared to traditional inspecting techniques, electrochemical biosensors supply many advantages such as heightened sensitivity,[24] non-invasive means of searching for biomolecules, and improved specificity. Moreover, it is worth noting that these biosensors exhibit little susceptibility to potential obstacles such as optical interference or sample turbidity.[25]

Electrochemical techniques are used to diagnose oral cancer by identifying certain biomarkers found in saliva. These biomarkers are categorized into three primary groups: DNA biosensors, RNA biosensors, and protein biosensors.[26]

Wu and colleagues created a dual 3D nanorobot that combines an ISAR-based DNA walker with a Cas12a-based nano-harvester. This nanorobot is designed to quickly and accurately identify salivary miRNA-31 with high sensitivity. The miRNA of interest is trapped by magnetic nanoparticles that have been modified with DNA hairpins. These nanoparticles then undergo a process called walking, facilitated by an ISAR-based walker, to form multiple DNA double helices. These helices are then combined with crRNA-Cas12a to create a 3D nano-harvester. The nano-harvester cuts and releases hairpin probes labeled with methylene blue from the sensing interface, leading to a noticeable change in the signal. The nano-harvester using Cas12a exhibits improved *trans*-cleavage efficiency. The detection of miRNA-31 in saliva samples demonstrates that this newly created biosensor is a rapid, highly sensitive, and very selective sensing platform. It has significant promise for the early diagnosis of oral squamous cell carcinoma (OSCC).[27]

Literature review indicated that, there is no investigation (research work) for the identification of micro-RNA-423-5p in human saliva samples using biosensor technique. In this study, an DNA-based biosensor was developed for the sensitive and specific monitoring of this biomarker by oligonucleotide hybridization. The analysis of the building phases of the constructed genosensor included the examination of many critical factors, including the hybridization time and the concentration of micro-RNA-423-5p. Subsequently, electrochemical techniques such as cyclic voltammetry (CV), chronoamperometry (ChA), and differential pulse voltammetry (DPV) were used to determine MicroRNA-423-5p in human real samples. The performance characteristics of the biosensor were assessed in terms of stability, repeatability, and suitability for use in plasma samples and collecting saliva.

For the opening a new horizon on the early-stage diagnosis of OC, a novel selective and sensitive electrochemical label-free biosensor was developed by using dendritic AuNPs-modified GCE (glassy carbon electrode), of poly(β-CD), and KCC-1-nPr-NH-Arg for the detection of MicroRNA-423-5p in human saliva samples. As far as we know, there has been no prior development of a biosensor specifically designed to detect MicroRNA-423-5p. Our research presents a groundbreaking synthesis technique, never explored before in the electrochemical synthesis of dendritic AuNPs, opening new strategy for future investigations. To manufacture a high-potential capturing layer, the surface of a GCE was automatically modified by poly-β-cyclodextrin (β-CD) using electropolymerization method. The synthesis and evaluation of KCC-1-nPr-NH-Arg nanoparticles were conducted with the specific aim of enhancing the surface-to-volume ratio of modified P (β-CD).

2. Experimental

2.1. Chemicals and reagents

βCD (M_w = 1134.98 g mol^{-1}) $C_{42}H_{70}O_{35}$, mercaptohexanol (MCH), cetyltrimethylammonium bromide (CTAB), hydrogen tetrachloroaurate (III) hydrate ($HAuCl_4$–$3H_2O$), potassium ferricyanide $K_3Fe(CN)_6$, potassium ferrocyanide $K_4Fe(CN)_6$, and sulfuric acid (98%), were purchased from Sigma-Aldrich. Fresh frozen plasma samples were obtained from the Iran Blood Transfusion Research Center (Tabriz, Iran). Phosphate-buffered saline (PBS) solutions with a concentration of 0.05 M were created for two different pH values, namely pH 4 (for polymerization purposes) and pH 7.4 (for bioanalysis). These solutions were prepared by dissolving Na_2HPO_4 (0.1 M) and NaH_2PO_4 (0.1 M) in deionized water. The procurement of deionized water was conducted by the Shahid Ghazi Pharmaceutical Company, Tabriz, Iran. The other reagents used in this investigation had an analytical grade. The target oligonucleotides (Table 1) used in this investigation were produced and purified through BioRP, a process conducted by Bioneer Co., Korea. The use of complementary DNA and microRNA was first employed to investigate the manufacture and optimization parameters of the electrode.

Human saliva samples were obtained from the Faculty of Dentistry (Tabriz University of Medical science, Tabriz, Iran, (Ethic code: IR.TBZMED.REC.1401.202)). All experiments were performed in accordance with the guidelines of institute (Tabriz University of Medical science), and approved by the ethics committee at Tabriz University of Medical science, Tabriz, Iran. Informed consents were obtained from human participants of this study. Saliva samples were collected in the fasting state (at least 8 hours have passed since the last eating and drinking). For this purpose, to ensure the cleanliness of the oral cavity before sampling, the oral cavity was rinsed using phosphate buffer (0.1 M) and pH = 7.4 for 30 seconds. After discarding the phosphate buffer, the oral cavity was rinsed with deionized water for 20 seconds. Finally, saliva samples were collected and used after ensuring clarity and absence of suspended particles.

2.2. Apparatus

The GCE surface underwent electrochemical modification using a standard three-electrode cell (from Metrohm, Barendrecht, Netherlands) run by an electrochemical system that featured an AUTOLAB system with PGSTAT302 N. A common three-electrode cell from Metrohm served as the evaluation tool for the electrochemical experiments. The working electrode was a GCE (d = 2 mm) (from Azar Electrode Co., West Azerbaijan, Iran); Pt wire worked as a counter electrode; and Ag/AgCl-saturated KCl was a reference electrode. The assembly was powered by a PalmSens electrochemical system with PSTrance 5.9 software as a running program (PS4.F1.05, Palm Instruments, Utrecht, The Netherlands). Techniques: CV and DPV with the following parameters: $T_{equilibration}$, 2 s; E_{begin}, −1.0 V; E_{end}, 1.0 V; E_{step}, 0.1 V; E_{pulse}, 0.1 V; t_{pulse}, 0.2 s; scan rate, 0.1 V s^{-1}; and ChA (for the deposition of gold nanoparticles onto a GCE) were used to investigate the electrochemical behavior of the designed genosensor. The chemical components present on the surface of the modified electrode were examined using energy-dispersive X-ray spectroscopy (EDX) using the MIRA3 TESCAN model, located in Brno, the Czech Republic. In addition, a field-emission scanning electron microscope (FE-SEM, Hitachi High-Technologies, Hitachi-Su8020, Praha, Czech Republic) was used to look at the shape of the electrode surface.

2.3. Pre-cleaning of the GCE electrode

To facilitate improvements, it was necessary to do a comprehensive cleaning of the bare GCE using both mechanical and electrochemical methods. In the process of mechanical cleaning, the electrodes underwent a 10 minutes polishing procedure on a velvet cloth that had been soaked in a liquid solution. Subsequently, the electrodes were subjected to a 10 minutes period of sonication in a mixture consisting of equal parts water and acetone. In the electrochemical process, the electrodes were submerged in a solution of sulfuric acid (0.1 M) and subjected to 10 cycles of the CV method. A scan rate of 0.1 V s^{-1} was used, spanning the voltage range from −0.5 to 1.2 V.

2.4. Electropolymerization of β-CD on the surface of the GCE

CDs possess a distinctive steric configuration of their glucose units, rendering them soluble in aqueous solutions. This property enables CDs to serve as significant complexation agents for a diverse array of hydrophobic molecules, including natural chemicals and plant bioactive. Consequently, CDs have gained prominence in both industrial and scientific domains. One notable benefit of incorporating lipophilic compounds into CDs is the augmentation of their water solubility, leading to improved stability and bioavailability of these guest molecules.[28]

A compelling option to the physically immobilized CD and the covalently coupled CD supramolecules is the electropolymerization of the CDs to produce a cohesive and insoluble CD polymer. While the CD supramolecules that are physically adsorbed onto the surface may dissolve and gradually detach,

Table 1 Oligonucleotide sequences of DNA probe, MicroRNA-423-5p (target), 2-base mismatch DNA, non-complement (MicroRNA-21)

Name	Sequences (5′ –> 3′)
MicroRNA-423-5p	UGAGGGGCAGAGAGCGAGACUUU
DNA probe	5′-SH-TGTCTCCCCGGTGTCTGGCTCGA-3′
2-Base mismatch DNA	TGGCTCCCCGGTGTCTGGTTCGA
Non-complement (MicroRNA-21)	TGTCGGGTTGCTGTCCTCTTC

resulting in a gradual decrease in CD concentration on the surface, the CD polymer that is insoluble remains attached. Furthermore, several investigations have shown the favorable conductive characteristics of this polymer, making it a very suitable contender for the advancement of electrochemical-based sensors.[29]

The CV technique was used to successfully electropolymerization β-CD onto the GCE surface. This electropolymerization process was conducted within a potential range of −2 to +2 V, including a total of 40 consecutive cycles (Fig. S1 (see ESI†)).

The CV technique was used to successfully electropolymerization βCD onto the GCE surface. This electropolymerization process was conducted within a potential range of −2 to +2 V, including a total of 40 consecutive cycles. In the first cycle, a cathodic peak (peak 1) was observed at the potential of 0.5 discernible. After the second cycle, the anodic peaks (peak 3) and (peak 2) occurred at 1.5 V and 0.5 V, respectively. As of the seventh cycle, a new cathodic peak (peak 4) appeared at −0.5 V. In the following cycles, the peak current increased, indicating the development of P (β-CD) on the CGE's surface. Furthermore, the current increased rapidly until cycle 28 and then progressively decreased in intensity in the following cycles, indicating that the polymeric film could have reached its maximum thickness.

The electropolymerization of β-CD consists of five distinct steps. The electropolymerization is begun by the oxidation of the monomer, resulting in the formation of a radical cation (**I**). In this scenario, it is feasible to amalgamate two monomers in their oxidized state to produce an oligomer, namely a dimer, which consists of two bound monomer units (**II**). The oligomer may undergo oxidation to generate a radical cation (**III**). This oxidized oligomer may react with a previously oxidized monomer to create another oligomer, namely a trimer consisting of three bonded monomer units (**IV**). Ultimately, the monomer units are added in a sequential manner to the active site, resulting in the formation of an expanding polymer chain (**V**). The interaction between the radical cations might take place *via* carbon–carbon bonds, nitrogen–nitrogen, or carbon–nitrogen.[30] The Scheme 1 illustrates the whole process of electropolymerization of β-CD.

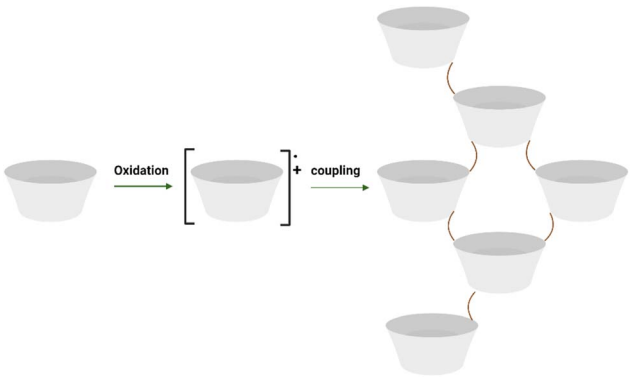

Scheme 1 Fundamental and significant mechanism of electropolymerization.

2.5. Synthesis process of KCC-1-nPr-NH-Arg

The synthesis procedure of KCC-1-nPr-NH-Arg was done based on our pervious report.[31] According to high surface to volume of KCC-1-nPr-NH-Arg (104.9 $m^2 g^{-1}$) and its ability to increment of DNA dense loading, this dendritic fibrous nanosilica (DFNS) was drop-cast on the surface of GCE-P(βCD). For this purpose, 0.001 g of KCC-1-nPr-NH-Arg was dissolution in PBS (0.1 M, pH = 7.4) and incubated at 37 °C for 24 h. Next, the solution was centrifuged fir 5 min with 6000 rpm. Then, the supernatant was removed. Then, 5 μL of proposed DFNS was drop-cast on the surface of GCE-P(βCD) and incubated in 4 °C for 6 h. Finally, the proposed electrode (P(βCD)-KCC-1-nPr-NH-Arg) was washed by DW and dry at room temperature.

2.6. Electrosynthesis of AuNPs with dendritic morphology

(AuNPs) with a variety of morphologies and forms, including nanorods, nanoclusters,[32] nanoflowers,[33] nano-stars,[34] nanocages,[35] nano-bipyramids,[36] and nanowires,[37] have been used as probes due to their exceptional qualities, which may be utilized to create biosensors *via* surface modification, AuNPs may detect particular targets either directly or indirectly *via* many processes, including but not limited to hydrogen bonding, nucleic acid hybridization,[38,39] aptamer-target binding, antigen–antibody recognition, enzyme inhibition, and enzyme-mimicking activity.[40]

Thiols have been shown to form self-assembled monolayers (SAMs) on the surface of gold electrode.[41] "Self-assembly" describes the haphazard creation of distinct nanometer-sized components from more basic subunits or building pieces. The most well-known SAMs are those of thiols and dithiols (and other S headgroup compounds, such as disulfides and sulfides) on various oxide-free metals and, to a lesser degree, on semiconductors, due to their potential and ongoing uses in multiple disciplines of nanotechnology.[42]

ChA technique was utilized for the generation of AuNPs with dendritic morphology on the surface of electrode. Fig. S2 (see ESI†) presents the ChA of deposition of AuNPs onto the GCE's modified P(βCD)-KCC-1-nPr-NH-Arg surface. This deposition process was conducted at a steady potential of 0 V for 300 seconds.[43]

GCE modified with P(β-CD)-KCC-1-nPr-NH-Arg has been transferred as the working electrode into the cell holding the Au nanoparticle solution. Following that, the electrodeposition was done using the ChA approach, with the following parameters: $T_{equilibration} = 2$ s, $E_{dc} = 0$ V, $t_{interval} = 0.1$ s, and $t_{run} = 300$ s.[43] CTAB and sulfuric acid were used in the synthesis of Au nanoparticles. After preparing a 10 mM "$HAuCl_4$–$3H_2O$" solution, 200 mM of sulfuric acid was used to dissolve 10% CTAB. Ultimately, the initially produced solution was mixed with 10 mM of the "$HAuCl_4$–$3H_2O$" solution (at a volume ratio of 1 : 1 : 1 V : V : V). To get a uniform solution, the vessel was softly shaken. The solution had an orange hue shift. To give the AuNPs nanoparticles with consistent shape and prevent them from

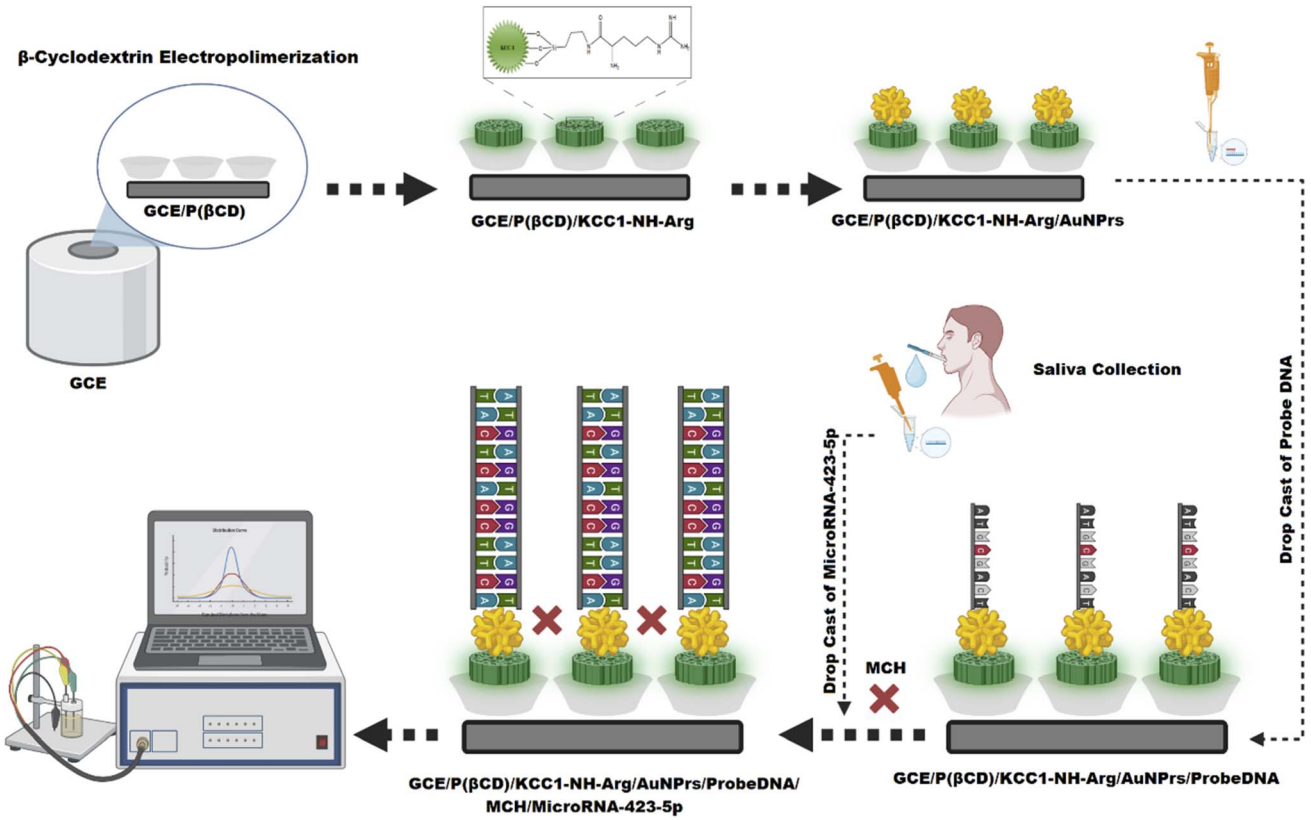

Scheme 2 The designed electrochemical genosensor fabrication process for MicroRNA-423-5p detection.

clumping together, a 10% CTAB solution was used as both a design and a sealant. Sulfuric acid was also employed as a solvent solution. Also, using this combination ($HAucl_4^-$, H_2SO_4, CTAB) and adjustment of electro-synthesis potential in 0 V, AuNPs with dendritic structure was obtained.

2.7. Fabrication of the electrochemical genosensor

In this step of biosensor fabrication, the proposed electrode (GCE-P(β-CD)-KCC-1-nPr-NH-Arg) was used to immobilization of DNA sequence. For this purpose, particular DNAs with the sequence 5′-SH-TGTCTCCCCGGTGTCTGGCTCGA-3′ were immobilized on the surface of GCE modified by P(β-CD)-KCC-1-nPr-NH-Arg-AuNPs for 12 hours at 4 °C (optimized incubation time). P(β-CD)-KCC-1-nPr-NH-Arg-AuNPs-probeDNA was exposed to 10 μL MCH, an effective blocker agent, for 30 minutes at 25 °C in order to inhibit the electrode's non-specific sites. Lastly, modified GCE was exposed to 10 μL of MicroRNA-423-5p for 30 minutes at 37 °C. Scheme 2 shows different steps of genosensor fabrication process.

3. Results and discussion

3.1. Characterization of different steps of sensor fabrication using FE-SEM and EDX

FE-SEM and EDX methods were utilized for the characterization of electrode surface in variation steps of biosensor construction. FE-SEM images of (A) P(β-CD), (B) P(β-CD)-KCC-1-nPr-NH-Arg, (C) P(β-CD)-KCC-1-nPr-NH-Arg-AuNPs, (D) P(β-CD)-KCC-1-nPr-NH-Arg-AuNPs-probeDNA, (E) P(β-CD)-KCC-1-nPr-NH-Arg-AuNPs-probeDNA-MCH-MicroRNA-423-5p were recorded at the same time. Fig. 1A shows FE-SEM image of GCE-P(β-CD), resulting in the formation of P(β-CD) with an ordered and well-organized interconnected architecture. P(β-CD) morphology provides a monodispersed spherical, homogeneous polymer film that is optimal for macromolecular transferring efficiencies. Fig. 1B shows FE-SEM image of KCC-1-nPr-NH-Arg stabilized on GCE-P(β-CD) surface. The morphology of the electrode surface is altered to a cylindrical shape, which confirms successful formulation of the KCC-1-nPr-NH-Arg on the surface of electrode. Also, Fig. 1C shows FE-SEM image of the formation of gold nanoparticles with dendritic morphology on the surface of electrode. Fig. 1D shows the FE-SEM after immobilization the specific sequence of DNA containing the thiol group on the surface of the GCE coated with AuNPs. Obtained result after immobilization the specific sequence containing the thiol group and creating a link between the thiol group and the gold nanoparticles (Au–S), the surface of the electrode has become spongy.

Fig. 1E shows the FE-SEM images of the GCE modified with P(β-CD)-KCC-1-nPr-NH-Arg-AuNPs after the hybridization of the DNA sequence with the complementary sequence of the target (microRNA-423-5p). It can be seen that the interaction of DNA with the target analyte has been done successfully, which

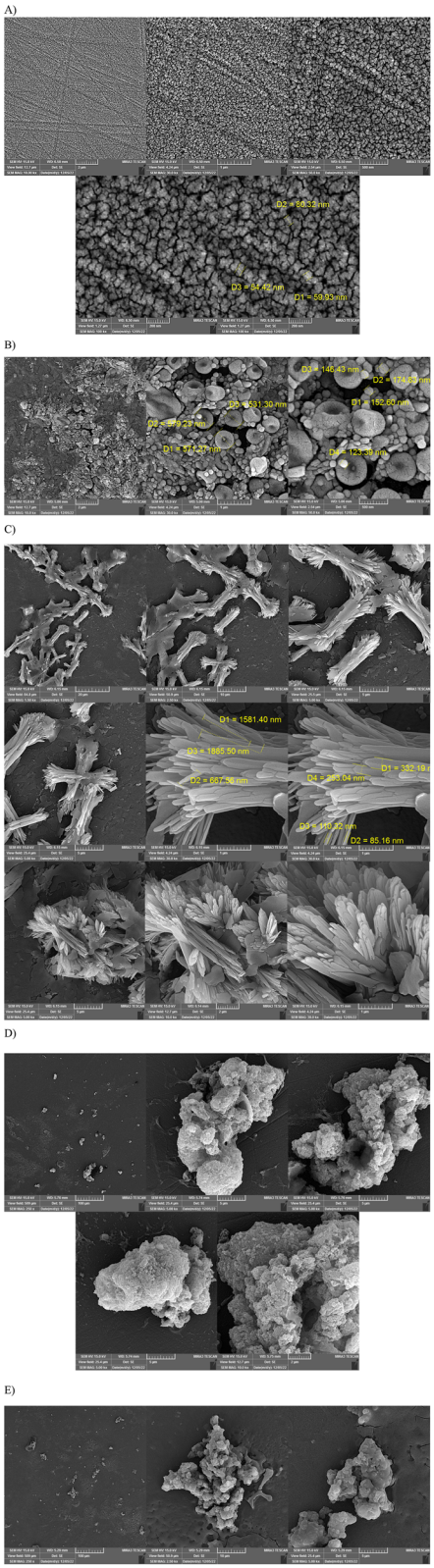

Fig. 1 FE-SEM images of (A) P(β-CD), (B) P(β-CD)-KCC-1-nPr-NH-Arg, (C) P(β-CD)-KCC-1-nPr-NH-Arg-AuNPs, (D) P(β-CD)-KCC-1-nPr-NH-Arg-AuNPs-probeDNA, (E) P(β-CD)-KCC-1-nPr-NH-Arg-AuNPs-probeDNA-MCH-MicroRNA-423-5p in different magnifications.

confirms the completion of the genosensor manufacturing process.

Also, EDX of electrode shows successful preparation of genosensor after different fabrication steps (Fig. S3 (see ESI†)).

3.2. Investigating the electrochemical behavior of the designed biosensor

CV and DPV techniques were used to inspect the electrochemical performance of the designed biosensor. To confirm the correctness of the biosensor preparation process, its CV was investigated in a $Fe(CN)_6^{-3/-4}$ (0.01 M) electrolyte solution containing 0.01 M KCL in the potential range of −1 to +1 V. After each step of electrode modification, voltammograms were recorded and compared. According to Fig. 2A, the CV shows an anodic peak current intensity of 32.08 μA and a cathodic peak current intensity of −35 μA for the GCE-P(β-CD) electrode. Next, with the addition of KCC-1-nPr-NH-Arg to the electrode surface, the intensity of the anodic current increases due to the presence of arginine on the structure of DFNS and its interaction with the surface, so that its numerical value reaches 45.28 μA. The addition of AuNPs to the structure of the current intensity sensor reaches to 48.13 μA, which confirms the successful deposition of gold nanoparticles.

According to Fig. 2A, a voltammogram with high anodic and cathodic peak current was obtained for the modified GCE, while for the electrode modified with the probe, the peak current due to the irregular accumulation of the thiolated probe on the electrode surface was significantly reduced, which slows down the electron transfer related to the oxidation and reduction process of $Fe(CN)_6^{-3/-4}$ on the surface of the GCE. In fact, single-stranded probes immobilized on the surface of the GCE (either in a suitable and correct orientation or with a non-specific orientation and with folded and deformed forms) from the presence of the electroactive compound $Fe(CN)_6^{-3/-4}$ is prevented on the surface of the electrode and the peak current of the anodic and cathodic is reduced.

In the continuation of the work, the effect of MCH on the arrangement of single-stranded probes immobilized on the surface of the electrode was investigated. To do this, after immobilizations the single-stranded probes on the electrode surface, the modified electrode was incubated in a 0.1 mM solution of MCH. In the presence of MCH solution, the redox signal related to of $Fe(CN)_6^{-3/-4}$ has increased due to the separation of single-stranded probes that are non-specifically and irregularly placed on the electrode surface.

Then the designed biosensor was incubated in a solution of target (microRNA-423-5p) for half an hour. According to obtained CVs, as a result of the hybridization process and the formation of double-stranded oligonucleotides (probe double strand with target microRNA), the anodic and cathodic peak current related to the oxidation and reduction processes of $Fe(CN)_6^{-3/-4}$ on the surface of the modified electrode were greatly reduced. In fact, the decrease in the signal of the anodic and cathodic processes was a good indication of the proper performance of the hybridization process at the level of the designed biosensor. So, the modified electrode with a self-

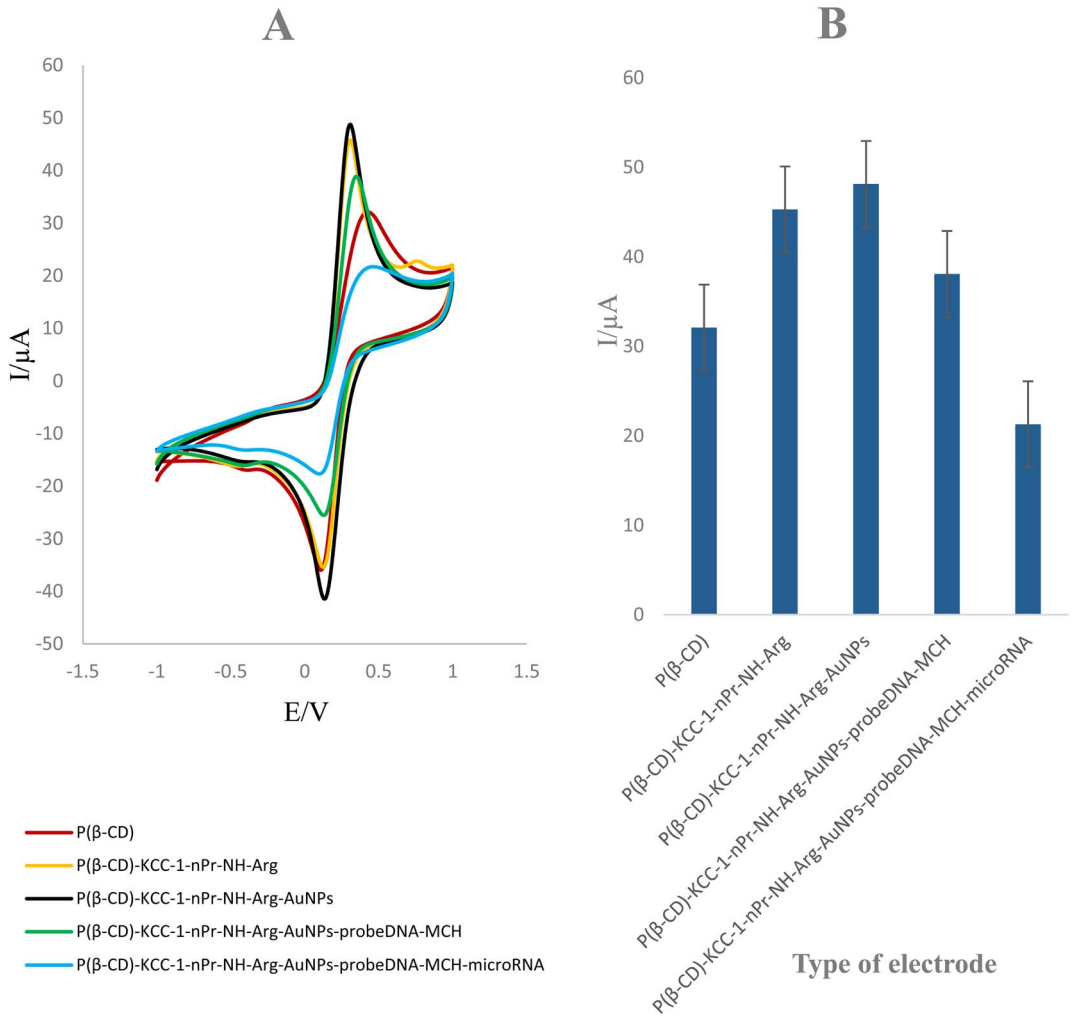

Fig. 2 (A) CVs of P(β-CD)-modified GCE, P(β-CD)-KCC-1-nPr-NH-Arg-modified GCE, P(β-CD)-KCC-1-nPr-NH-Arg-AuNPs-modified GCE, P(β-CD)-KCC-1-nPr-NH-Arg-AuNPs-probeDNA-MCH-modified GCE, P(β-CD)-KCC-1-nPr-NH-Arg-AuNPs-probeDNA-MCH-microRNA-modified GCE in 0.01 M $Fe(CN)_6^{-3/-4}$ and 0.01 M KCl as the supporting electrolyte with a sweep rate of 100 mV s^{-1}. (B) Bar-graph of changes in peak current at different stages of genosensor fabrication.

arranged single-strand probe can be used to perform the hybridization process.

The interpretation of the decrease in anodic and cathodic peak current intensity in the voltammograms can be expressed as follows: immobilizations of single-stranded oligonucleotide probes, as well as the accumulation of hybridized double-stranded oligonucleotides, which have a negatively charged phosphate agent in their chain, as an inhibitory layer, result from the presence of the electroactive anionic compound $Fe(CN)_6^{-3/-4}$, which has a negative charge. As a result, the intensity of the current decreases, and the oxidation of the electrode is greatly reduced.

In addition to the substantial decrease in the intensity of the oxidation peak current and reduction of the electrode in the presence of $Fe(CN)_6^{-3/-4}$, it can be seen that with the increase in the presence of oligonucleotides, both single-stranded and non-arranged single-stranded probes, as well as hybridized double-stranded probes on the surface of the electrode, the anodic and cathodic peaks of the mentioned voltammograms have moved to more positive and negative potential values, respectively. This observation indicates that due to the presence of oligonucleotides on the surface of the electrode, the redox process of the compound $Fe(CN)_6^{-3/-4}$ has become more difficult due to the creation of steric hindrance and the presence of the negative charge of oligonucleotides, and as a result, the oxidation and reduction potentials are shifted towards larger values.

The comparison results of the present voltammograms confirm the correct performance of various steps during the fabrication of the electrochemical biosensor and show the ability of the sensor regarding the hybridization process target microRNA detection.

DPV is exactly according to the process obtained in CV and the results are as follows: Fig. S4 (see ESI†). For the GCE-P(β-CD) conductive electrode, the peak current is 14.10 μA. After adding mesoporous nano-silica, this value reaches to 52.96 μA. The maximum value of current intensity is obtained by depositing AuNPs, which was 84.34 μA. By adding the target microRNA

(microRNA-423-5p), the peak current decreased to 11.21 μA, which confirms the hybridization of the target analyte (microRNA-423-5p).

3.3. Analytical studies (standard sample)

After modifying the electrode surface, 5 μL of single-strand DNA probe with a concentration of 1 nM was dropped on the electrode surface for stabilization and hybridization. After immobilizations of the DNA single strand, the oxidation peak current of $Fe(CN)_6^{-3/-4}$ that accumulated on the electrode surface was measured using the DPV technique (Fig. S5 (see ESI†)). The above steps were carried out for concentrations of (0.1, 0.05, 0.01, and 0.001 nM) of a single-stranded analyte (microRNA-423-5p).

The regression equation in the range of 0.001 nM to 1 nM is as follows:

$$I(\mu A) = 3.3829 \ln C_{microRNA} + 29.73,\ R^2 = 0.9567$$

Its sensitivity is 3.3829 μA nM^{-1} with LLOQ = 0.001 nM.

According to the obtained results, there is a linear relation between peak current of calibration curve and Napierian Logarithm of microRNA-423-5p concentration. So, it is possible to determine low level of microRNA-423-5p in standard samples. Based on these results, engineered biosensor is able to determine in real samples that spiked by microRNA-423-5p.

3.3.1. Analytical studies in real samples (human blood plasma). The performance of sensor was studied to identify microRNA-423-5p in human plasma samples. 100 μL of human plasma samples were diluted in 900 μL of deionized water, and certain amounts of microRNA were added to them. The DPV technique was chosen as a sensitive diagnostic method (Fig. 3).

Blood was drawn from a 30 year-old healthy non-cancerous individual, collected in an additive-free sample storage tube, and allowed to clot for 60 minutes at room temperature to separate serum from blood. After that, it spent a night at 4 °C. The samples were twice centrifuged, first at 150 *g* for 5 minutes and again at 350 *g* for 15 minutes. To inactivate the proteins, the separated serum was collected in a tube containing 0.2 M EDTA solution. Following that, the tubes were often rotated a few times, the samples were separated into equal portions, and they were kept in storage at −20 °C. Freeze-thaw cycles were avoided and fresh or temporarily kept serum (up to three days) was the sole material used for all actual sample experiments. Blood sampling was done from a volunteer who was fully conscious of the purpose of blood sampling. Furthermore, the experiment met with all relevant laws and procedures, and blood sample was carried out in accordance with normal ethical principles.

The regression equation in the concentration range of 0.005 nM to 1 nM of microRNA-423-5p is as follows:

$$I(\mu A) = -5.8127 \ln C_{microRNA} + 17.084,\ R^2 = 0.996$$

Its sensitivity is 5.8127 μA $(ng\ L)^{-1}$ with LLOQ = 0.005 nM. According to the obtained results, there is a linear relation between peak current of calibration curve and Napierian Logarithm of microRNA-423-5p concentration. So, it is possible to determine low level of microRNA-423-5p in standard samples. Based on these results, engineered biosensor is able to non-invasive determination of microRNA-423-5p in real samples (human blood plasma).

3.3.2. Analytical studies in real samples (healthy saliva sample). Investigations of sensor performance were performed to detect microRNA-423-5p in healthy human saliva samples. Unprocessed human saliva samples were used as real samples for early-stage OC detection. Saliva samples were collected in the fasting state (at least 8 hours have passed since the last eating and drinking). For this purpose, to ensure the cleanliness of the oral cavity before sampling, the oral cavity was rinsed using phosphate buffer (0.1 M) and pH = 7.4 for 30 seconds. After discarding the phosphate buffer, the oral cavity was rinsed with deionized water for 20 seconds. Finally, saliva samples were collected and used after ensuring clarity and absence of suspended particles.

The DPV technique was chosen as a sensitive diagnostic method (Fig. 4). In this part, 100 μL of human healthy saliva samples were diluted in 900 μL of deionized water and then analyte was added to it in concentrations range of 1, 0.05, 0.01, 0.001 nM. Next, voltammograms were recorded.

The regression equation in the range of 0.001 nM to 1 nM is as follows:

$$I(\mu A) = -6.9137 \ln C_{microRNA} + 12.239,\ R^2 = 0.9183$$

Its sensitivity is 6.9137 μA $(ng\ L)^{-1}$ with LLOQ = 0.001 nM.

According to the obtained results, there is a linear relation between peak current of calibration curve and Napierian Logarithm of microRNA-423-5p concentration. So, it is possible to determine low level of microRNA-423-5p in standard samples. Based on these results, engineered biosensor is able to non-invasive determination of microRNA-423-5p in saliva sample of patient of OC.

3.3.3. The results of the genosensor performance in patient samples (oral cancer sample). Investigations of sensor performance were performed to detect microRNA-423-5p in human saliva samples with OC. The DPV technique was chosen as a sensitive diagnostic method (Fig. S6 (see ESI†)). In this section, the drop-casting process of cancerous saliva was performed with the incubated genosensor and DPV was recorded.

Cancerous saliva samples obtained from four people with OC along with a healthy person's saliva sample were used as a control to check the performance of the genosensor. Then DPVs of each of them was recorded and repeated 3 times (Fig. S6 (see ESI†)).

The obtained results prove that since there is no microRNA-423-5p in the control sample, the peak of its DPV current intensity graph has increased and reached to 16 μA which indicates the absence of hybridization with the DNA probe.

Unlike the control sample, microRNA-423-5p is present in human saliva samples with OC, and due to hybridization with the DNA probe, the DPV peak current intensity has decreased

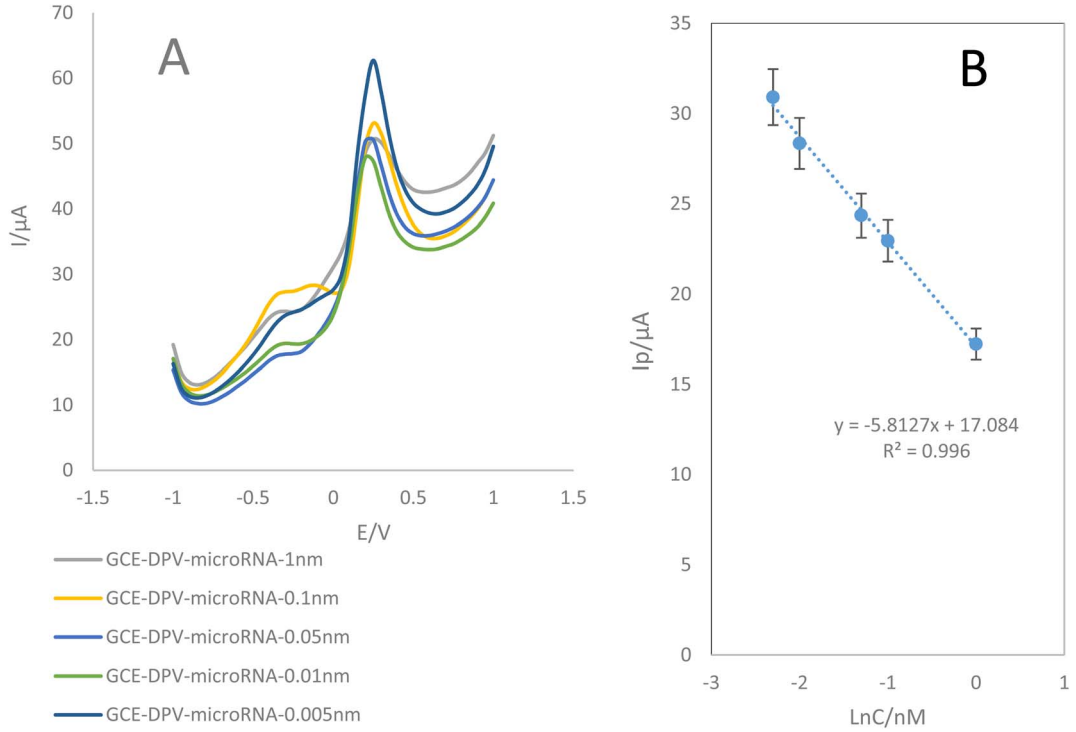

Fig. 3 (A) DPVs of the genosensor in different concentrations of microRNA-423-5p: 1, 0.1, 0.05, 0.01, 0.005 nM with treated human plasma sample in 0.01 M $Fe(CN)_6^{-3/-4}$ and 0.01 M KCl as the supporting electrolyte with a sweep rate of 100 mV s^{-1} (B) calibration curve against the concentration value microRNA in untreated human plasma samples.

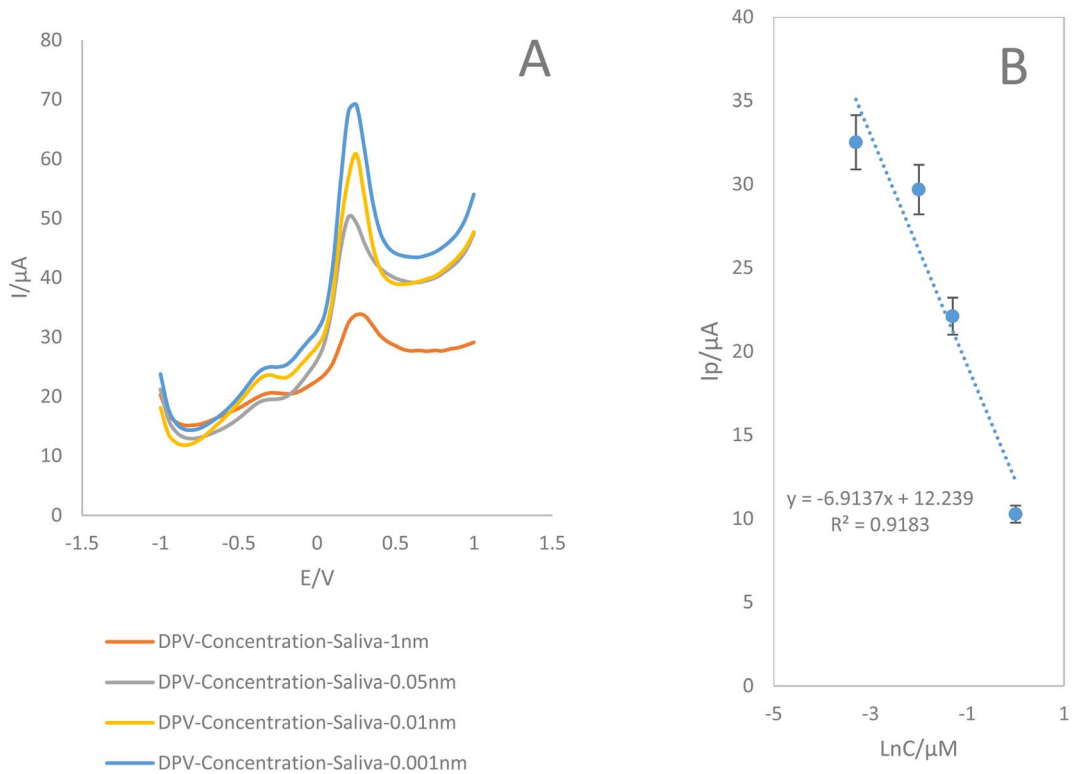

Fig. 4 (A) DPVs of the constructed genosensor in different concentrations of microRNA-423-5p: 1, 0.05, 0.01, 0.001 nM with healthy human saliva samples in 0.01 M $Fe(CN)_6^{-3/-4}$ and 0.01 M KCl as the supporting electrolyte with a sweep rate of 100 mV s^{-1} (B) Calibration curve *versus* the amount of microRNA concentration in saliva samples of healthy human.

for all four cancerous saliva samples, and it varies between 2-6 μA.

A paired *t*-test was performed to check the significance of the data using SPSS Statistics version 20.0 software. With all of the tested drugs, apart from aspirin ($p = 0.042$), no statistically significant differences ($p < 0.05$) were obtained between the responses Accuracy shows the closeness of the results obtained from a method after several repetitions which expressed based on the percentage of relative standard deviation (% RSD). For biological samples according to the FDA standard, a % RSD of up to 15% is acceptable.

The RSD obtained for cancer samples is as follows, which confirms the success of this step: cancer-control (SD average = 7.74)

3.4. Selectivity of the genosensor

To check the specificity of the prepared biosensor, DPVs of the genosensor were recorded in the presence of $Fe(CN)_6^{-3/-4}$ electrolyte solution (0.1 M) containing KCl in the potential range of −1 up to +1 V. Also, DPVs of the genosensor were recorded in the presence of ncDNA and 2-base mismatch sequences (Fig. 5).

According to the obtained results, it was found that the sensor prepared in the presence of the target analyte has a current intensity distinguishable from ncDNA and 2-base mismatch DNA, which indicates the selectivity of the relevant electrochemical biosensor. The peak current obtained for the target sequence was equal to 11 μA. While for ncDNA, the obtained peak current intensity was about 20 μA. Also, for 2-base mismatch, the obtained peak current intensity value is twice different from the obtained peak current intensity value for ncDNA, and it shows the selectivity of the engineered genosensor.

3.5. Repeatability of the fabricated substrate

To check the repeatability and calculate the average peak current and the RSD of the constructed genosensor for two minimum and maximum concentrations of the target analyte, three repetitions were performed by the DPV technique (Fig S7 and Table S1 (see ESI†)). The numerical value of the RSD for the minimum concentration is 0.3616, and for the maximum concentration, it was 3.24865.

The low value of the obtained RSD shows the optimal repeatability of the present biosensor and therefore confirms its efficiency in reliable measurements in different samples. In addition to this, the ease and repeatability of the biosensor manufacturing process is one of its very important and valuable advantages.

3.6. Evaluation of the stability

3.6.1. Inter-day stability. One of the most important aspects of biosensor functionality that needs ongoing observation is stability. Surface stability of a P(β-CD)-KCC-1-nPr-NH-Arg-modified GCE was tested by CV technique in the presence of 0.01 M $Fe(CN)_6^{-3/-4}$ and 0.01 M KCl as the supporting electrolyte with a sweep rate of 100 mV s^{-1} (Fig. S8 (see ESI†)).

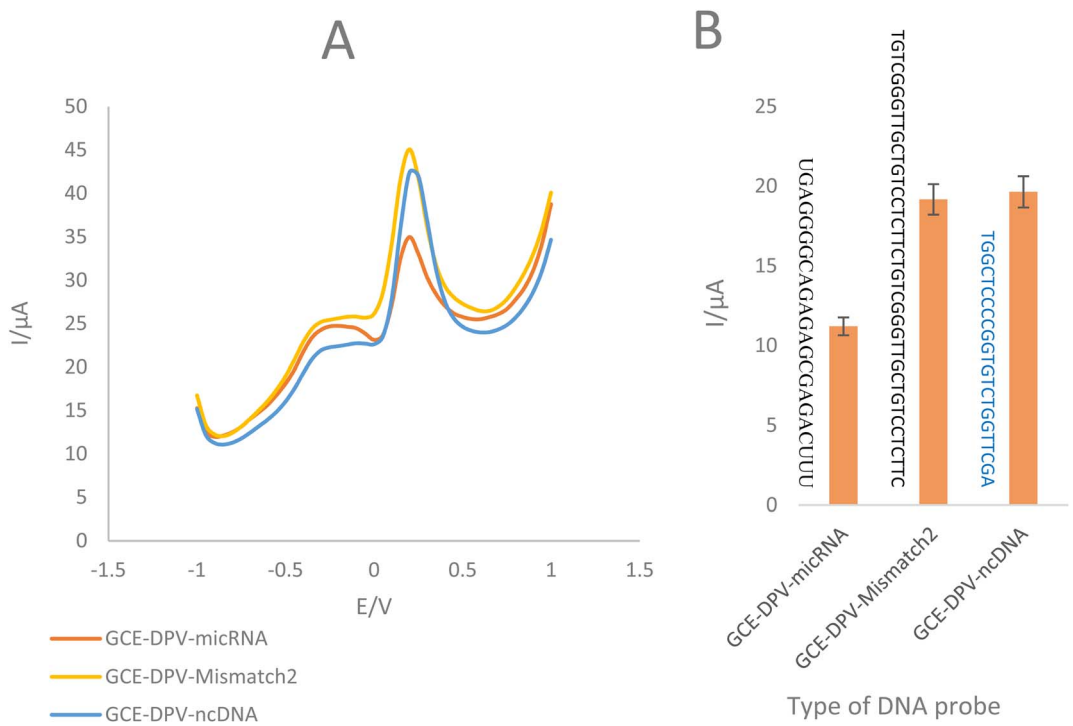

Fig. 5 (A) DPVs of the biosensor recorded for target complementary sequence and non-complementary sequences in 0.01 M $Fe(CN)_6^{-3/-4}$ and 1 0.0 M KCl as the supporting electrolyte with a sweep rate of 100 mV s^{-1} (B) Histogram of peak current intensity *versus* different type of DNA sequences.

According to the obtained results, until the fourth day, the CV peak current intensity is about 50 μA, and from the fifth day on, the electrode substrate lost its stability and reached to 41 μA, which shows the stability of the electrode for four days.

3.6.2. Intra-day stability. To that end, the stability of the designed biosensor substrate (P(β-CD)-KCC-1-nPr-NH-Arg-modified GCE) was examined during a two-hour within 30 minutes' period (Fig. S9 (see ESI†)). Checking the stability of the internalization of the GCE surface was done every half hour. According to Fig. S9 (see ESI†), for up to two and a half hours, the CV current intensity was about 42 μA. From the third hour onwards, the electrode substrate lost its stability and reached to 36 μA, which shows the two-and-a-half-hour stability of the electrode surface. Therefore, as soon as this genosensor is manufactured, it should be put to use.

3.6.3. Cyclic stability. A voltammogram of the P(β-CD)-KCC-1-nPr-NH-Arg-modified GCE matrix has been recorded for 10 continuous cycles, since the stability of this matrix on the electrode surface throughout successive measurements may provide some indication of the stability of the genosensor (Fig. S10 (see ESI†)). According to the obtained results, the intensity of the peak current after 10 full cycles of the CV decreases to 34 μA, which indicates a decrease in the stability of the substrate to repeat its use. Therefore, it is suggested that the utilized inter face can be reused up to 5 cycles.

3.7. Kinetic study

The scan rate is a crucial factor to consider when assessing redox reactions for the purpose of analyte identification. The redox behavior of $Fe(CN)_6^{-3/-4}$/KCl was studied using the GCE-P(βCD)-KCC-1-nPr-NH-Arg electrode.

The CVs of electrode was recoded in different sweep rates (0.2, 0.15, 0.1, 0.09, 0.07, 0.06, 0.05 mV s^{-1}). Based on the acquired CV graph (Fig. S11A (see ESI†)), an increase in scan rate led to a gradual widening of the voltammogram and a considerable change in the anodic peak current. Electrons are very likely to transfer at the interface of the electrode, resulting in the increment of a peak current. This process happens more slowly when the scan rates are reduced. Also, Fig. 5B demonstrates that there is a direct correlation between the scan rate, ranging from 0.2 to 0.05 mV s^{-1}, and the peak current. This correlation suggests that the diffusion process is responsible for controlling mass-transfer.

Two commonly used methods to investigate the reversibility of reactions and determine whether a reaction is regulated by diffusion or adsorption include analyzing the dependencies: I_p *vs.* $v^{0.5}$ and $\ln I_p$ *vs.* $\ln v$. Fig. S11C and D (see ESI†) shows these trends for the oxidation peak. If there are no kinetic complexities in reversible or irreversible systems, the values of I_p and $v^{0.5}$ are linked and intersect at the origin of the figure. Fig. S11C (see ESI†) clearly demonstrates that the I_{pa} and $v^{0.5}$ curve is linear, with a high coefficient of determination ($R^2 = 0.9958$), and intersects the origin. This relationship is described by the following equation:

$$I_{pa}\ (\mu A) = -166.07v^{0.5}\ (V\ s^{-1})^{0.5} - 1.3373\ (R^2 = 0.9958)$$

The relationship between these variables originates from the origin, suggesting that the kinetic process of electron transfer is controlled by diffusion.

The dependency between $\ln I_{pa}$ and $\ln v$ (Fig. S11D (see ESI†)) is linear throughout the chosen sweep rate range of 0.05 to 0.2 mV s^{-1}. This may be explained using the following equation:

$$\ln I_{pa}\ (\mu A) = 0.027157 \ln v\ (mV\ s^{-1}) + 117.96\ (R^2 = 0.9989)$$

Its slope is 0.027157 and exhibits diffusion-control of the electrode process. Diffusion-controlled systems are predicted to have slopes close to 0.5, while adsorption-controlled systems are predicted to have slopes near to 1.

The relationship between E_{pa} (anodic peak potential) and sweep rate is seen in Fig. S11E (see ESI†). Irreversible electrochemical reactions exhibit independence between the E_{pa} and sweep rate. This suggests that the electron transfer in these reactions is irreversible, since increasing the sweep rate leads to a rise in E_{pa}.

4. Conclusion

In summary, the P(βCD)-KCC-1-nPr-NH-Arg-AuNPs-probeDNA modified GCE demonstrated efficient detection of microRNA-423-5p, as indicated by ROC curve data. This study introduced the first reported drop casting of KCC-1-nPr-NH-Arg on the surface of GCE-P(βCD). So, we presented a novel electrochemical synthesis of dendritic AuNPs, serving as the current amplification component and providing a suitable surface for probe DNA insertion. Utilizing a DNA hybridizing strategy with a complementary probe sequence, we achieved non-invasive, rapid, and sensitive detection of microRNA-423-5p in biological samples, resulting in a detectable change in current. The electrocatalytic properties of the polymeric interface were evaluated using CV, DPV, and ChA methods. Under optimal conditions, the developed genosensor exhibited a suitable LLOQ of 1 pM and a wide linear detection range from 1 pM to 1 nM. These advantages position the constructed biosensors as promising tools for detecting microRNA in various biofluids, thus opening new horizons for the early-stage diagnosis of OC.

Data availability

Access to the data used in this study is available upon request and may be subject to approval by the data provider. Restrictions may apply to the availability of these data, which were used under license for this study. Interested parties are encouraged to contact the corresponding author for further information on accessing the data. All relevant data supporting the findings of this study are available within the article and its ESI† files, or from the corresponding author upon reasonable request. Access to some data may be restricted due to privacy or ethical restrictions. Any restrictions to data availability will be disclosed at the time of data request.

Conflicts of interest

There are no conflicts to declare.

Acknowledgements

This work was supported by TBZMED (Tabriz University of Medical Sciences)-Grant Number 67521-IR.TBZMED.REC.1401.202.

References

1 V. Borse, A. N. Konwar and P. Buragohain, Oral cancer diagnosis and perspectives in India, *Sens. Int.*, 2020, **1**, 100046.
2 D. M. Ghalwash, Diagnostic and prognostic value of salivary biomarkers in oral cancer and precancer, *J. Oral Maxillofac. Surg. Med. Pathol.*, 2020, **32**, 538–543.
3 F. T. Deutsch, S. J. Khoury, J. B. Sunwoo, M. S. Elliott and N. T. Tran, Application of salivary noncoding microRNAs for the diagnosis of oral cancers, *Head Neck*, 2020, **42**, 3072–3083.
4 R. M. Shanti, T. Tanaka and D. C. Stanton, Oral biopsy techniques, *Dermatol. Clin.*, 2020, **38**, 421–427.
5 F. Lousada-Fernandez, O. Rapado-Gonzalez, J.-L. Lopez-Cedrun, R. Lopez-Lopez, L. Muinelo-Romay and M. M. Suarez-Cunqueiro, Liquid biopsy in oral cancer, *Int. J. Mol. Sci.*, 2018, **19**, 1704.
6 S. Mazumder, S. Datta, J. G. Ray, K. Chaudhuri and R. Chatterjee, Liquid biopsy: miRNA as a potential biomarker in oral cancer, *Cancer Epidemiol.*, 2019, **58**, 137–145.
7 M. Idrees, C. S. Farah, P. Sloan and O. Kujan, Oral brush biopsy using liquid-based cytology is a reliable tool for oral cancer screening: A cost-utility analysis, *Cancer Cytopathol.*, 2022, **130**, 740–748.
8 D. Maraghelli, M. Pietragalla, L. Calistri, L. Barbato, L. G. Locatello, M. Orlandi, N. Landini, A. Lo Casto and C. Nardi, Techniques, tricks, and stratagems of oral cavity computed tomography and magnetic resonance imaging, *Appl. Sci.*, 2022, **12**, 1473.
9 P. Thoenissen, A. M. Bucher, A. Heselich, R. Sader, T. Vogl and S. Ghanaati, Evaluation of Flap Shrinkage Using Magnetic Resonance Imaging Follow-up in the Treatment of Oral Cancer, *J. Reconstr. Microsurg. Open*, 2023, **8**, e12–e17.
10 E. Terzidis, J. Friborg, I. R. Vogelius, G. Lelkaitis, C. von Buchwald, A. B. Olin, H. H. Johannesen, B. M. Fischer, I. Wessel and J. H. Rasmussen, Tumor volume definitions in head and neck squamous cell carcinoma–Comparing PET/MRI and histopathology, *Radiother. Oncol.*, 2023, **180**, 109484.
11 T. Iwai, S. Ishikawa, Y. Ideta, S. Sugiyama, Y. Hayashi, S. Minamiyama, H. Kitajima and K. Mitsudo, Limitation of PET/CT for screening of synchronous upper gastrointestinal cancer in oral cancer patients, *J. Oral Maxillofac. Surg. Med. Pathol.*, 2023, **36**(2), 191–194.
12 R. Mahieu, D. N. Donders, G. C. Krijger, F. T. Ververs, R. de Roos, J. L. Bemelmans, R. van Rooij, R. de Bree and B. de Keizer, Within-patient comparison between [68Ga] Ga-tilmanocept PET/CT lymphoscintigraphy and [99mTc] Tc-tilmanocept lymphoscintigraphy for sentinel lymph node detection in oral cancer: a pilot study, *Eur. J. Nucl. Med. Mol. Imaging*, 2022, **49**, 2023–2036.
13 D. R. Schwaninger, M. Hüllner, D. Bichsel, B. Giacomelli-Hiestand, N. S. Stutzmann, P. Balermpas, S. Valdec and B. Stadlinger, FDG-PET/CT for oral focus assessment in head and neck cancer patients, *Clin. Oral Investig.*, 2022, **26**, 4407–4418.
14 Y.-T. Lin, S. Darvishi, A. Preet, T.-Y. Huang, S.-H. Lin, H. H. Girault, L. Wang and T.-E. Lin, A Review: Electrochemical Biosensors for Oral Cancer, *Chemosensors*, 2020, **8**, 54.
15 E. G. Park, H. Ha, D. H. Lee, W. R. Kim, Y. J. Lee, W. H. Bae and H.-S. Kim, Genomic Analyses of Non-Coding RNAs Overlapping Transposable Elements and Its Implication to Human Diseases, *Int. J. Mol. Sci.*, 2022, **23**, 8950.
16 T. M. Al-Noshokaty, A. Mansour, R. Abdelhamid, N. Abdellatif, A. Alaaeldien, T. Reda, N. M. Abdelmaksoud, A. S. Doghish, A. I. Abulsoud and S. S. Elshaer, Role of long non-coding RNAs in pancreatic cancer pathogenesis and treatment resistance-A review, *Pathol., Res. Pract.*, 2023, 154438.
17 J. S. Mattick, P. P. Amaral, P. Carninci, S. Carpenter, H. Y. Chang, L.-L. Chen, R. Chen, C. Dean, M. E. Dinger and K. A. Fitzgerald, Long non-coding RNAs: definitions, functions, challenges and recommendations, *Nat. Rev. Mol. Cell Biol.*, 2023, **24**, 430–447.
18 L. Erfanparast, M. Taghizadieh and A. A. Shekarchi, Non-coding RNAs and oral cancer: small molecules with big functions, *Front. Oncol.*, 2022, **12**, 914593.
19 R. Shang, S. Lee, G. Senavirathne and E. C. Lai, microRNAs in action: biogenesis, function and regulation, *Nat. Rev. Genet.*, 2023, 1–18.
20 J. Rodríguez-Molinero, B. del Carmen Migueláñez-Medrán, E. Delgado-Somolinos, C. M. Carreras-Presas and A. F. López-Sánchez, Advances in the Diagnosis, Monitoring, and Progression of Oral Cancer through Saliva: An Update, *BioMed Res. Int.*, 2022, **2022**, 2739869.
21 C. Romani, E. Salviato, A. Paderno, L. Zanotti, A. Ravaggi, A. Deganello, G. Berretti, T. Gualtieri, S. Marchini and M. D'Incalci, Genome-wide study of salivary miRNAs identifies miR-423-5p as promising diagnostic and prognostic biomarker in oral squamous cell carcinoma, *Theranostics*, 2021, **11**, 2987.
22 F. S. Nahm, Receiver operating characteristic curve: overview and practical use for clinicians, *Korean J. Anesthesiol.*, 2022, **75**, 25–36.
23 M. Negahdary and L. Angnes, Application of electrochemical biosensors for the detection of microRNAs (miRNAs) related to cancer, *Coord. Chem. Rev.*, 2022, **464**, 214565.
24 Y. Hui, Z. Huang, M. E. E. Alahi, A. Nag, S. Feng and S. C. Mukhopadhyay, Recent advancements in

electrochemical biosensors for monitoring the water quality, *Biosensors*, 2022, **12**, 551.

25 Y.-T. Lin, S. Darvishi, A. Preet, T.-Y. Huang, S.-H. Lin, H. H. Girault, L. Wang and T.-E. Lin, A review: Electrochemical biosensors for oral cancer, *Chemosensors*, 2020, **8**, 54.

26 E. Ahmadian, S. M. Dizaj, S. Sharifi, S. Shahi, R. Khalilov, A. Eftekhari and M. Hasanzadeh, The potential of nanomaterials in theranostics of oral squamous cell carcinoma: Recent progress, *TrAC, Trends Anal. Chem.*, 2019, **116**, 167–176.

27 Y. Wu, J. Pei, Y. Li, G. Wang, L. Li, J. Liu and G. Tian, High-sensitive and rapid electrochemical detection of miRNA-31 in saliva using Cas12a-based 3D nano-harvester with improved *trans*-cleavage efficiency, *Talanta*, 2024, **266**, 125066.

28 S. Wüpper, K. Lüersen and G. Rimbach, Cyclodextrins, natural compounds, and plant bioactives—a nutritional perspective, *Biomol. Ther.*, 2021, **11**, 401.

29 B. Healy, T. Yu, D. C. da Silva Alves, C. Okeke and C. B. Breslin, Cyclodextrins as supramolecular recognition systems: Applications in the fabrication of electrochemical sensors, *Materials*, 2021, **14**, 1668.

30 A. C. Pereira, A. E. F. Oliveira and G. B. Bettio, β-Cyclodextrin electropolymerization: Mechanism, electrochemical behavior, and optimization, *Chem. Pap.*, 2019, **73**, 1795–1804.

31 N. Hasannezhad and N. Shadjou, KCC-1-nPr-NH-Arg as an efficient organo-nanocatalyst for the green synthesis of 1, 8-dioxo decahydroacridine derivatives, *J. Mol. Recognit.*, 2022, **35**, e2956.

32 W. Cheng, C. Duan, Y. Chen, D. Li, Z. Hou, Y. Yao, J. Jiao and Y. Xiang, Highly sensitive aptasensor for detecting cancerous exosomes based on clover-like gold nanoclusters, *Anal. Chem.*, 2022, **95**, 3606–3612.

33 K. E. Rogers, O. K. Nag, K. Susumu, E. Oh and J. B. Delehanty, Photothermal-Enhanced Modulation of Cellular Membrane Potential Using Long-Wavelength-Activated Gold Nanoflowers, *Bioconjugate Chem.*, 2023, **34**, 405–413.

34 C. Fernández-Lodeiro, J. Fernández-Lodeiro, A. Fernández-Lodeiro, S. Nuti, C. Lodeiro, A. LaGrow, I. Pérez-Juste, J. Pérez-Juste and I. Pastoriza-Santos, Synthesis of tuneable gold nanostars: the role of adenosine monophosphate, *J. Mater. Chem. C*, 2023, **11**, 12626–12636.

35 W. Xiao, Y. Xiong, Y. Li, Z. Chen and H. Li, Non-Enzymatically Colorimetric Bilirubin Sensing Based on the Catalytic Structure Disruption of Gold Nanocages, *Sensors*, 2023, **23**, 2969.

36 P. T. Huynh, K. T. Le Tran, T. T. H. Nguyen, V. Q. Lam, N. T. K. Phan and T. V. K. Ngo, Preparation and characterization of spiked gold nanobipyramids and its antibacterial effect on methicillin-resistant Staphylococcus aureus and methicillin-sensitive Staphylococcus aureus, *J. Genet. Eng. Biotechnol.*, 2023, **21**, 1–11.

37 G. Pelayo-Punzano, R. Jurado, M. López-Haro, R. Cuesta, J. J. Calvino, J. M. Domínguez-Vera and N. Gálvez, Gold nanoparticle-coated apoferritin conductive nanowires, *RSC Adv.*, 2023, **13**, 19420–19428.

38 E. Eksin and A. Erdem, Recent progress on optical biosensors developed for nucleic acid detection related to infectious viral diseases, *Micromachines*, 2023, **14**, 295.

39 S. Shi, J. Chen, X. Wang, M. Xiao, A. R. Chandrasekaran, L. Li, C. Yi and H. Pei, Biointerface Engineering with Nucleic Acid Materials for Biosensing Applications, *Adv. Funct. Mater.*, 2022, **32**, 2201069.

40 Z. Hua, T. Yu, D. Liu and Y. Xianyu, Recent advances in gold nanoparticles-based biosensors for food safety detection, *Biosens. Bioelectron.*, 2021, **179**, 113076.

41 R. Marie, H. Jensenius, J. Thaysen, C. B. Christensen and A. Boisen, Adsorption kinetics and mechanical properties of thiol-modified DNA-oligos on gold investigated by microcantilever sensors, *Ultramicroscopy*, 2002, **91**, 29–36.

42 C. Vericat, M. Vela, G. Benitez, P. Carro and R. Salvarezza, Self-assembled monolayers of thiols and dithiols on gold: new challenges for a well-known system, *Chem. Soc. Rev.*, 2010, **39**, 1805–1834.

43 R. D. Vais, N. Sattarahmady and H. Heli, Green electrodeposition of gold nanostructures by diverse size, shape, and electrochemical activity, *Gold Bull.*, 2016, **49**, 95–102.